nature geoscience

ARTICLES

https://doi.org/10.1038/s41561-019-0420-9

West Antarctic ice loss influenced by internal climate variability and anthropogenic forcing

Paul R. Holland[1*], Thomas J. Bracegirdle[1], Pierre Dutrieux[2], Adrian Jenkins[1] and Eric J. Steig[3]

Recent ice loss from the West Antarctic Ice Sheet has been caused by ocean melting of ice shelves in the Amundsen Sea. Eastward wind anomalies at the shelf break enhance the import of warm Circumpolar Deep Water onto the Amundsen Sea continental shelf, which creates transient melting anomalies with an approximately decadal period. No anthropogenic influence on this process has been established. Here, we combine observations and climate model simulations to suggest that increased greenhouse gas forcing caused shelf-break winds to transition from mean easterlies in the 1920s to the near-zero mean zonal winds of the present day. Strong internal climate variability, primarily linked to the tropical Pacific, is superimposed on this forced trend. We infer that the Amundsen Sea experienced decadal ocean variability throughout the twentieth century, with warm anomalies gradually becoming more prevalent, offering a credible explanation for the ongoing ice loss. Existing climate model projections show that strong future greenhouse gas forcing creates persistent mean westerly shelf-break winds by 2100, suggesting a further enhancement of warm ocean anomalies. These wind changes are weaker under a scenario in which greenhouse gas concentrations are stabilized.

The West Antarctic Ice Sheet (WAIS) has been losing ice throughout the satellite record, currently at a rate equivalent to global sea-level rise of ~4.5 cm century^{-1} (2012–2017 average)[1]. This ice loss is known to be driven by changes in ocean melting of ice shelves[2], but it remains unclear whether these changes can be attributed to contemporary climate change. The rate of ice loss shows large variations[3,4] driven by decadal variability in oceanic conditions[5,6]. However, this ocean variability does not necessarily explain the overall ice loss, as on longer timescales the WAIS could be in balance with decadally varying forcing[7]. There is evidence that historical ocean melting anomalies caused ice streams to unground from stabilizing seabed features, triggering geometrical ice and ocean feedbacks that remain active[6,8–12]. In this study, we consider the possibility that the decadal variability is superimposed on a longer-term trend, increasing the mean melt rates about which decadal variations occur.

Warm Circumpolar Deep Water (CDW) has occupied the Amundsen Sea continental shelf since the earliest observations[13], but the thickness of the CDW layer varies markedly, driving the decadal variability in melting[6,14]. Observational and modelling evidence shows that the transport of CDW onto the Amundsen Sea shelf is strongly affected by ocean surface stresses at the shelf break[5,6,14–18]. By modifying the barotropic ocean flow, eastward stress anomalies enhance an undercurrent that transports CDW on-shelf via seabed troughs, thickening the CDW layer and increasing melting[5,18,19]. Additional processes such as local sea-ice growth and wind forcing modify ocean conditions over the shelf[20–22]. However, these surface processes have less influence at greater depths, which dominate variability in ice-shelf melting, and on longer timescales, which are of greatest importance to the ice-sheet response[7]. Furthermore, local surface processes can only reduce or re-distribute the ocean heat on the shelf; CDW import is the only process that can increase the overall on-shelf heat content. As a result, the observed history of ice-shelf melting shows a close correspondence to the import of CDW onto the shelf, which is regulated by zonal surface stresses over the shelf break[5,6]. This study relies on this established linkage between winds and ice-shelf melting and examines the wider drivers of wind anomalies, including tropical Pacific linkages, twentieth-century variability, the role of anthropogenic forcing and future projections.

Tropical Pacific forcing of Amundsen Sea variability

We estimate the total ocean surface stress on the Amundsen Sea, accounting for the effect of sea ice, by combining wind data from the European Centre for Medium-Range Weather Forecasts (ECMWF) Interim Reanalysis (ERA-Interim) with satellite-tracked sea-ice drift observations (Methods)[23]. The Amundsen Sea shelf break sits near the centre of the Amundsen Sea Low[24], where the long-term mean zonal stress is negligible (Fig. 1a). Interannual stress variability is large (Fig. 1b), and its uniformity across the region implies that shelf-break stresses experience exceptionally high variability relative to their low mean. This may explain why strong ocean (and ice-sheet) variability occurs in the Amundsen Sea.

Total stress and wind-only stress differ substantially over the shelf, but are highly correlated at the shelf break (Supplementary Fig. 1). Therefore, throughout this study we use zonal winds over the Pine Island/Thwaites Troughs (PITT; Fig. 1a) as a proxy for zonal stress and hence CDW transport onto the shelf. PITT winds contain anomalies with an approximately decadal period (Fig. 2a), which dominate the variability in ice-sheet forcing[5,6]. To focus on this variability, we hereafter apply a 2 yr running mean to all quantities, isolating decadal anomalies while preserving their extrema (Supplementary Fig. 2).

Maps of correlation between PITT winds and global sea surface temperature (SST) and sea-level pressure (SLP) are shown in Fig. 2b and Supplementary Fig. 3. Eastward wind anomalies are associated with weakening of the Amundsen Sea Low, part of a global response to anomalies in the tropical Pacific that is transmitted by standing atmospheric Rossby waves[9,25]. The global wind anomalies induce accompanying global SST anomalies by altering Ekman transport

[1]British Antarctic Survey, Cambridge, UK. [2]Lamont-Doherty Earth Observatory of Columbia University, Palisades, NY, USA. [3]Department of Earth and Space Sciences, University of Washington, Seattle, WA, USA. *e-mail: p.holland@bas.ac.uk

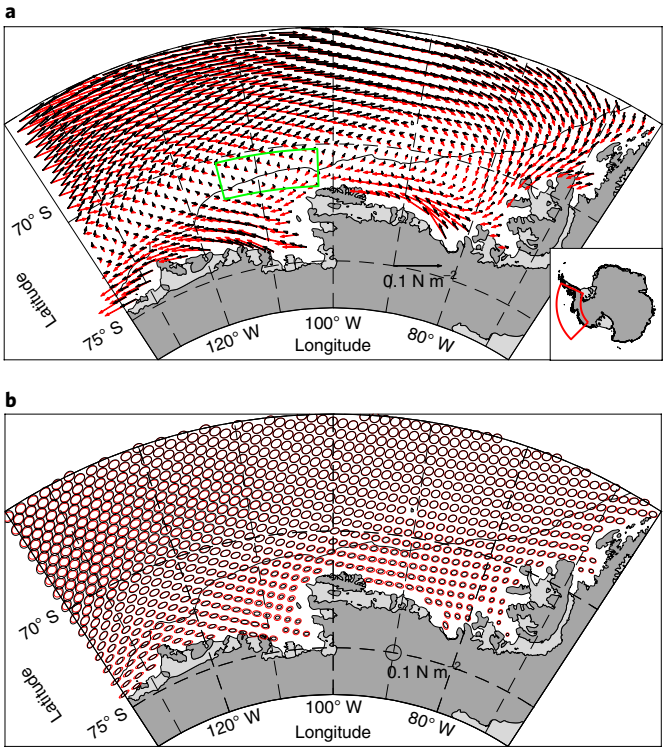

Fig. 1 | Total surface stress and wind-only stress on the Amundsen Sea. **a**, Mean 1992–2016 total stress (accounting for sea ice; black) and wind-only stress (red). **b**, Variance ellipses for monthly total and wind-only stress anomalies from seasonal climatology, aligned in the direction of maximum variance and scaled to 1 s.d. Vectors and ellipses are shown every second data point. The 1,000 m depth contour at the shelf break is also shown. The green box shows the PITT area at the shelf break, over which time series are calculated.

and surface fluxes[26]. Figure 2 also shows the Southern Oscillation Index (SOI), which represents the El Niño–Southern Oscillation, and the Interdecadal Pacific Oscillation (IPO) tripole index, which represents decadal Pacific variability (Methods). PITT winds are highly correlated with these indices, which represent natural variability that is internally generated within the climate system. Indeed, PITT wind anomalies are highly correlated to all measures of tropical Pacific variability[9,14] and bear no relation to other climate indices (Supplementary Fig. 4).

The strong statistical link between PITT winds and tropical Pacific SSTs provides an opportunity to constrain historical wind forcing of the Amundsen Sea, because tropical Pacific SSTs have been adequately observed since the 1920s (ref. [26]). To utilize these observations, we use an ensemble of 'pacemaker' climate model simulations[27] (PACE) to estimate PITT winds during the twentieth century (Methods). PACE comprises 20 simulations of the Community Earth System Model (CESM) under natural and anthropogenic radiative forcings, but is also constrained to follow observed tropical Pacific SST anomalies since 1920. This constraint ensures that the model winds follow the real history of the internal climate variability that is associated with the tropical Pacific. Since Pacific variability has such a strong influence on the Amundsen Sea, these simulations provide a constrained estimate of historical variability in PITT winds.

Each simulation within the PACE ensemble represents a single realization of the climate, so the real winds can be considered as being comparable to an individual ensemble member. The mean and variability of PITT winds in the PACE simulations compare very favourably with ERA-Interim (Fig. 3a). The PACE ensemble mean represents the mean trajectory of PITT winds under the real historical radiative forcing and tropical Pacific SST evolution. This ensemble mean is arguably the best-available reconstruction of historical PITT winds, since it averages over multiple realizations of the unknown internal climate variability associated with regions outside the tropical Pacific. Model correlation maps (Supplementary Fig. 5) confirm that the PACE ensemble-mean winds follow the processes seen in the observations.

The PACE ensemble-mean PITT winds show a general eastward trend of ~0.7 ms^{-1} $century^{-1}$ (Table 1). It also features eastward wind anomalies in 1940, the 1950s, 1970 and 1980 onwards (Fig. 3a) that are consistent with the glacial history inferred from sediments[12] and remote-sensing observations[3,4,8]. These linked wind and glacial anomalies are explored further below. The wind history is also supported by water-isotope ratios from West Antarctic ice cores, which show an increasing trend during the twentieth century and anomalously high values in response to the major El Niño of the early 1940s (refs. [28,29]).

The role of anthropogenic forcing

The PACE ensemble mean contains both a radiatively forced trend and the mean influence of internal variability associated with the tropical Pacific. We separate these by estimating the radiatively forced trend from the CESM Large Ensemble[30] (LENS; Methods). LENS uses the same model as PACE but without tropical SST restoring, providing 40 different realizations of internal climate variability from all sources, Pacific and otherwise (Fig. 3c). Taking the ensemble mean of LENS averages out this random internal variability, isolating the radiatively forced trend. The LENS ensemble mean has a PITT zonal wind trend of ~0.5 $m\,s^{-1}$ $century^{-1}$ during 1920–2005 (Table 1). Taken together, the CESM simulations (LENS and PACE) therefore imply that a forced wind trend removed a mean easterly PITT wind of ~0.5 $m\,s^{-1}$ that existed during the 1920s, to arrive at the present near-zero mean zonal winds (Fig. 3a). Acceleration of the southern subpolar westerlies is a well-known consequence of the meridional structure of radiatively forced atmospheric warming[31,32]. Our results show that this trend includes the latitude of PITT winds (Fig. 4a), despite the low correlation between the subpolar westerlies and PITT winds on interannual timescales (see the Southern Annular Mode in Supplementary Figs. 2 and 4).

The PITT region is highly sensitive to the modelled pattern of trends in the subpolar westerlies[31]. The wider ensemble of climate models contributing to the Coupled Model Intercomparison Project phase 5 (CMIP5; Methods) includes a variety of historical trends. The CMIP5 ensemble has no mean trend (Table 1), so the CESM is an outlier in this regard. However, the CMIP5 simulations have large biases in mean PITT winds relative to ERA-Interim (Fig. 4b and Supplementary Table 1), and the simulations with a smaller bias have a larger historical trend. The CESM simulations have an exceptionally small bias in mean PITT winds, providing support for their relatively large historical trends.

To formally separate tropical Pacific variability from the radiatively forced trend, we combine the PACE and LENS ensembles. As described above, the LENS ensemble mean represents the radiatively forced trend, while the PACE ensemble mean represents the radiatively forced trend plus the real tropical Pacific variability. Therefore, to isolate the influence of Pacific variability, we subtract the LENS ensemble mean ('forced response') from the PACE ensemble mean ('full response') to leave the 'tropical response'[27], that is, the influence of tropical Pacific SST restoring (Fig. 3b). Tropical response winds closely follow the unfiltered IPO index (Methods), implying multidecadal variability in PITT winds (for example, filtered IPO in Fig. 3b) that may be of great importance to the ongoing WAIS ice loss[7]. Comparing the PACE ensemble mean to the tropical response further illustrates the impact of the forced trend. The variability has

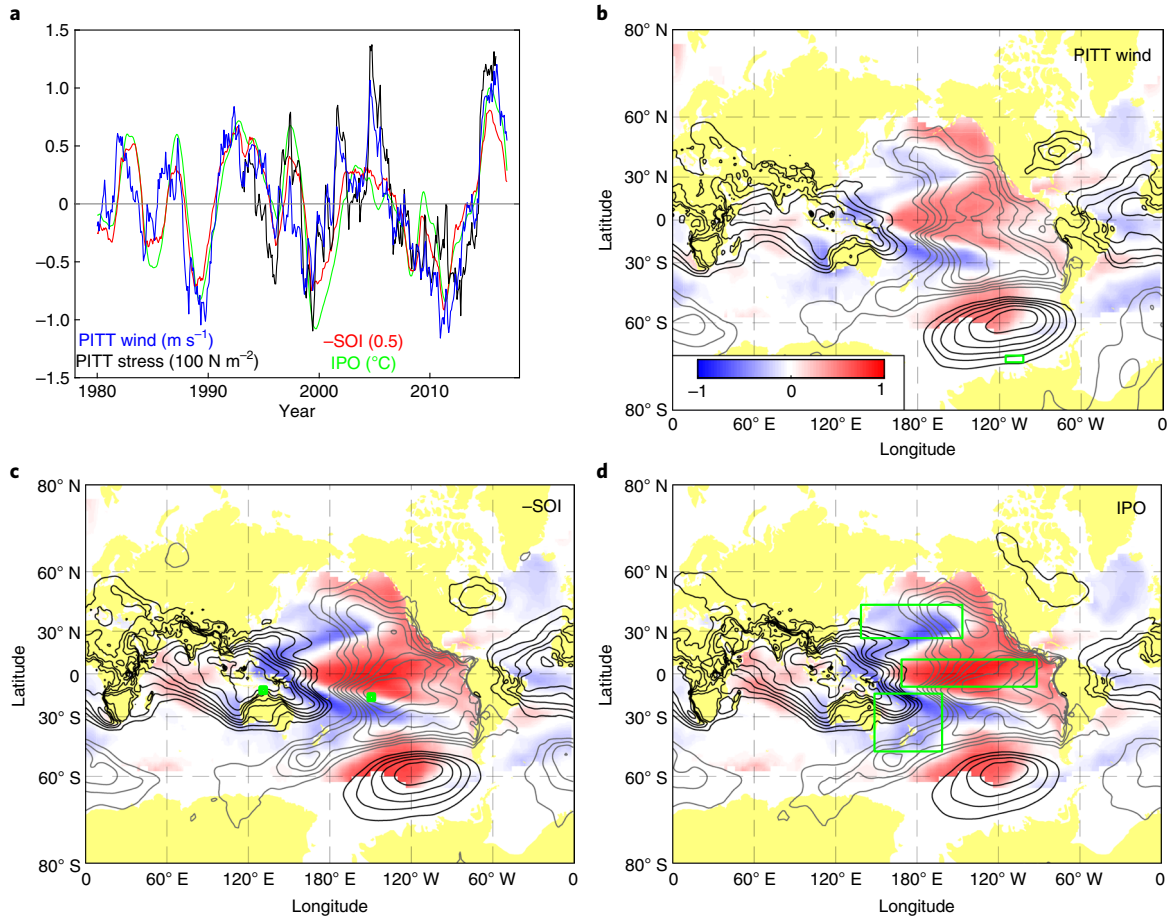

Fig. 2 | Linkages between Amundsen Sea winds and global SST and SLP. a, Time series of zonal wind and zonal total stress over the PITT box, the SOI and the IPO. The legend shows the unit for each time series, and scaling for the axis values where appropriate. **b**–**d**, Correlation maps of SST (colour) and SLP (contours) to PITT winds and SOI and IPO indices. The maps show r^2 multiplied by the sign of the relationship. SLP correlation contours have a spacing of 0.1, with black positive, grey negative and the zero contour omitted. The area of each index is outlined by green boxes.

not changed appreciably during the twentieth century (Fig. 3b), but absolute westerly wind anomalies that were rare have become commonplace (Fig. 3a). Given the strong evidence for a positive relationship between zonal wind anomalies and CDW import, this implies that warm anomalies in the Amundsen Sea have become progressively more prevalent through the twentieth century as a result of radiative forcing.

Radiative forcing has several sources, both anthropogenic (greenhouse gases, ozone, aerosols, land use) and natural (volcanoes, solar). The LENS ensemble mean represents the net effect of all sources, and additional simulations would be required to formally isolate the anthropogenic contribution. However, previous work has shown that forced trends in the southern subpolar westerlies are dominated by anthropogenic influences[33–35]. In contrast, there is no conclusive evidence that Pacific variability has been significantly affected by anthropogenic forcing[36,37]. Therefore, the evidence suggests that the forced trend in PITT winds is primarily anthropogenic in origin, while the influence of the tropical Pacific is primarily natural.

Implications for the WAIS

This analysis of the climate model ensembles offers a plausible narrative for the ongoing WAIS ice loss. (1) In the 1920s, the WAIS was closer to balance with cooler Amundsen Sea conditions associated with mean easterly PITT winds. (2) Through the twentieth century, the mean easterlies were progressively weakened by anthropogenic radiative forcing, causing tropically forced decadal warm ocean anomalies to become more prevalent at the ice-sheet margin. (3) Episodes of particularly strong eastward wind anomalies, for example, around 1940 (refs. [28,29]), created strong melting anomalies that caused ice streams to unground from seabed ridges, prompting progressive retreat as a result of ice and ocean feedbacks[10,11]. (4) As warm anomalies became more prevalent in recent decades, the ice-sheet imbalance was exacerbated, reaching the present-day rate.

Figure 5 illustrates this narrative by comparing PACE ensemble-mean winds to the glaciological evidence. Prominent eastward wind anomalies around 1940 and 1970 are consistent with the dates of initial and final ungrounding of Pine Island Glacier (PIG) from a seabed ridge inferred from sediment records and remote sensing[8,12]. Since 1980, eastward wind anomalies have triggered accelerations in glacial discharge[3] that induced drawdown of inland ice[4]. These eastward anomalies reflect Pacific variability that is not at all unusual in the record (Fig. 3b). However, when superimposed on the anthropogenic trend, this variability produces periods of absolute westerly winds that are sufficiently anomalous to account for much of the current ice loss.

This narrative proposes that present-day ice loss is driven by an anthropogenically forced melting imbalance modulated by natural tropical variability and ice–ocean feedbacks. The WAIS lost mass during recent warm ocean anomalies, but did not gain mass during

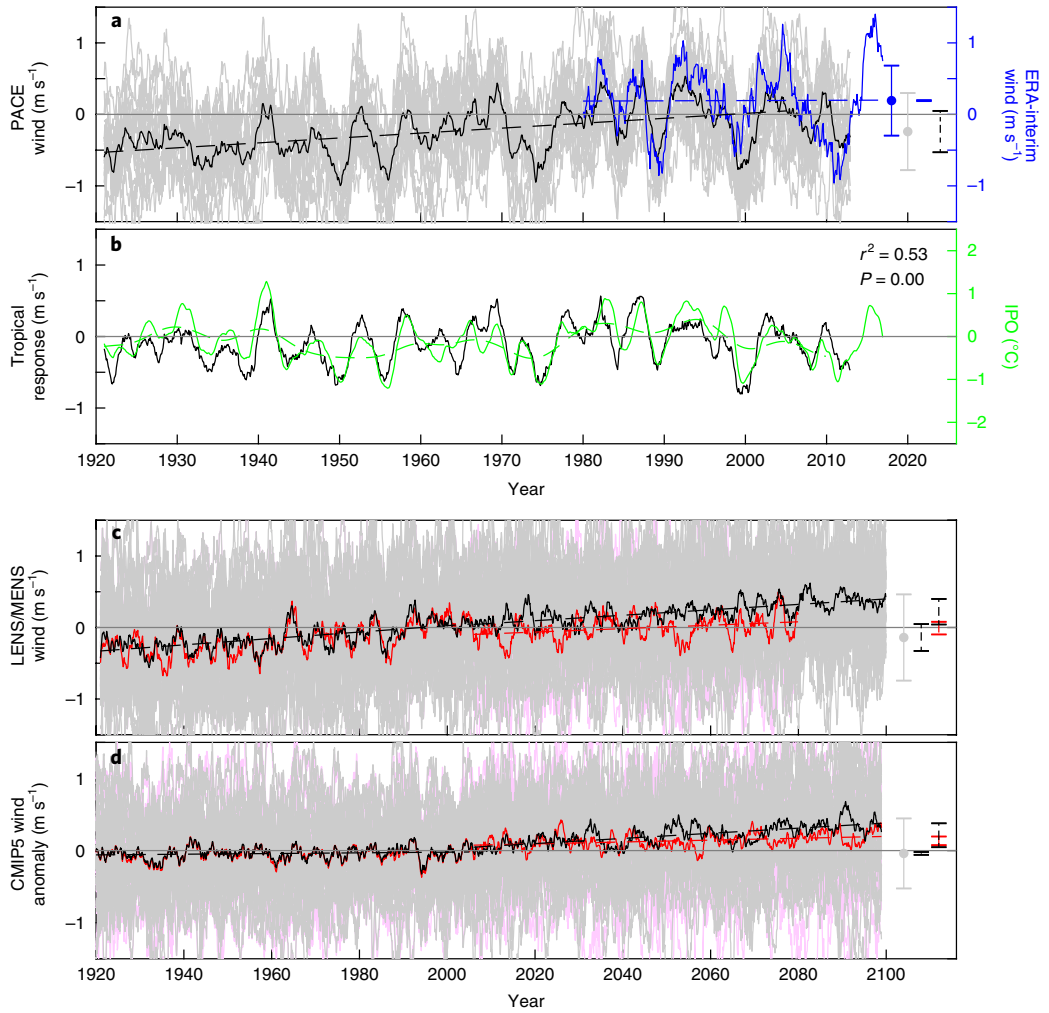

Fig. 3 | Amundsen Sea winds within climate model ensembles. a, Zonal winds over the PITT box from ERA-Interim (blue), PACE simulations (grey), PACE ensemble mean (black) and mean trend (dashed). **b**, 'Tropical response' wind (black) and IPO index before (green) and after (dashed) 13 yr low-pass filter. **c**, Historical and projection simulations of LENS (grey/black; RCP8.5) and MENS (pink/red; RCP4.5) ensembles. **d**, CMIP5 ensemble, including RCP8.5 (grey/black) and RCP4.5 (pink/red). Error bars show the standard deviation of wind anomalies (solid) and the magnitude of historical and projected trends (dashed). CMIP5 models contain large biases, so **d** shows anomalies from the 1979–2017 mean.

cool anomalies[3,4,6,38], an asymmetry that is consistent with both ice–ocean feedbacks and with the ice sheet being historically in balance with cooler ocean conditions. However, we caution that other narratives cannot yet be discounted, including those based solely on long-term natural variability in ice-sheet dynamics and climate forcing (for example, the IPO).

The unknown timing and magnitude of internal variability—other than that related to the tropical Pacific—adds considerable uncertainty to the actual trend in PITT winds over the twentieth century. All PACE simulations are equally plausible, and the standard deviation of PACE trends is nearly half the mean trend (Table 1 and Supplementary Fig. 6). In addition, the centennial trends are much smaller than decadal internal variability. In observations and CESM simulations, the ~0.5 m s^{-1} variability has equivalent magnitude to ~100 yr of the mean forced trends (Table 1 and Fig. 3). Decadal internal variability therefore dominates ice-sheet and ocean variability during the modern observational era (since 1979), and will continue to dominate observations for decades to come.

While weaker than decadal variability on short timescales, on centennial timescales we suggest that the wind trend is sufficiently large to have influenced ice-sheet stability. Recent PIG ice-shelf melting anomalies of ~40 Gt yr^{-1} are associated with PACE ensemble-mean wind anomalies of ~1.5 m s^{-1} (Fig. 5). If this ratio held for centennial trends, the PACE mean trend of ~0.7 m s^{-1} century^{-1} would induce a melting trend of ~20 Gt yr^{-1} century^{-1}. Integrated over 100 yr, this is half the magnitude of the decadal melting anomalies that affect ice-sheet mass balance (Fig. 5). Furthermore, PIG discharge was ~80 Gt yr^{-1} in 1974 (ref. [3]). If half was accounted for by melting[39], the integrated centennial trend would represent a 50% increase in melting over the 1974 rate. This simple argument supports the importance of the wind trends, but the centennial relationship between winds and melting remains a topic of considerable uncertainty that requires much further research.

Future projections

The historical PITT wind trend continues through the twenty-first century for the high-emissions representative concentration pathway 8.5 (RCP8.5) scenario, with LENS and CMIP5 projecting a mean trend of ~0.4 m s^{-1} century^{-1} (Table 1 and Figs. 3 and 4c). This suggests that warmer Amundsen Sea conditions will become progressively more prevalent. By 2100, the mean westerly is comparable to 1 s.d. of the internal variability, so the wind is reliably westerly (Table 1). The total 1920–2100 wind change is equivalent

Table 1 | Variability and trends in Amundsen Sea winds in the climate model ensembles

	Wind variability: s.d. of residuals from linear trends ($m\,s^{-1}$)	Wind trend: mean ±1 s.d. of trends in ensemble members ($m\,s^{-1}$ century^{-1})
ERA-Interim 1979–2016	0.49	0.04
PACE historical 1920–2005	0.54	**0.69 ± 0.27**
LENS historical 1920–2005	0.60	**0.45 ± 0.35**
CMIP5 historical 1920–2005	0.49	0.05 ± 0.36
MENS RCP4.5 2006–2080	0.59	**0.24 ± 0.27**
LENS RCP8.5 2006–2100	0.58	**0.38 ± 0.29**
CMIP5 RCP4.5 2006–2100	0.48	0.13 ± 0.47
CMIP5 RCP8.5 2006–2100	0.48	**0.36 ± 0.48**

Variability in PITT winds is characterized by the s.d. of residuals from the linear trends in all ensemble members. Note that the time series have a 2 yr running mean applied. Trends are characterized by the mean and s.d. of the distribution of linear trends in the ensemble members. Mean trends in bold are significantly different from zero at the 99% confidence level under a one-sample *t*-test. CMIP5 historical and CMIP5 RCP4.5 projected mean trends are not significant at the 90% level.

to ~2 s.d. of the internal variability, so if the WAIS were close to balance with ocean conditions in the 1920s, this suggests substantial ice-sheet change by 2100.

As described above, radiative forcing impacts in this region are dominated by anthropogenic influences, primarily ozone depletion and greenhouse gases[33–35]. Thirty-year wind trends within the CESM centennial records (Supplementary Fig. 7) show elevated trends centred on the 1980s and reduced trends centred on 2030 that represent the influence of ozone depletion and recovery. In the RCP8.5 scenario, the effect of ozone depletion causes only a temporary perturbation to the underlying trend, caused by greenhouse gases, that persists throughout the twentieth and twenty-first centuries.

Of course, twenty-first century radiative forcing is not decided. Under RCP4.5, CMIP5 simulations project PITT wind trends that are not significantly different from zero (Table 1, Figs. 3d and 4c, and Supplementary Fig. 6) because ozone recovery fully compensates the weaker greenhouse gas forcing in this scenario[40]. The difference between CMIP5 RCP4.5 and RCP8.5 wind trends is significant at the 95% confidence level (Supplementary Tables 2 and 3). Alternative evidence can be gained by comparing the LENS RCP8.5 projection to the CESM Medium Ensemble (MENS; ref. [41]), a 15-member ensemble of RCP4.5 projections (Methods). The 2006–2080 MENS mean projected wind trend is lower than that of LENS, but unlike the CMIP5 results this difference is not statistically significant (Supplementary Tables 2 and 3).

The CMIP5 RCP4.5/8.5 comparison samples a range of model responses to radiative forcing, while the LENS/MENS comparison better characterizes the role of internal variability, in a model with exceptionally low mean-state bias. Overall, these results suggest that weaker wind trends under RCP4.5 lead to Amundsen Sea ocean conditions frequently cooler than under RCP8.5. RCP4.5 and RCP8.5 scenarios differ in a specific subset of anthropogenic forcings (greenhouse gases, aerosols, land use), suggesting that policymakers have an opportunity to 'weight the dice' towards a lower future sea-level contribution from the WAIS. This conclusion relates to ocean changes induced by wind forcing, the mode of variability that has dominated observations[5,6]. The future contribution of additional warming mechanisms, such as a general warming of the CDW entering the Amundsen Sea, is highly uncertain[42].

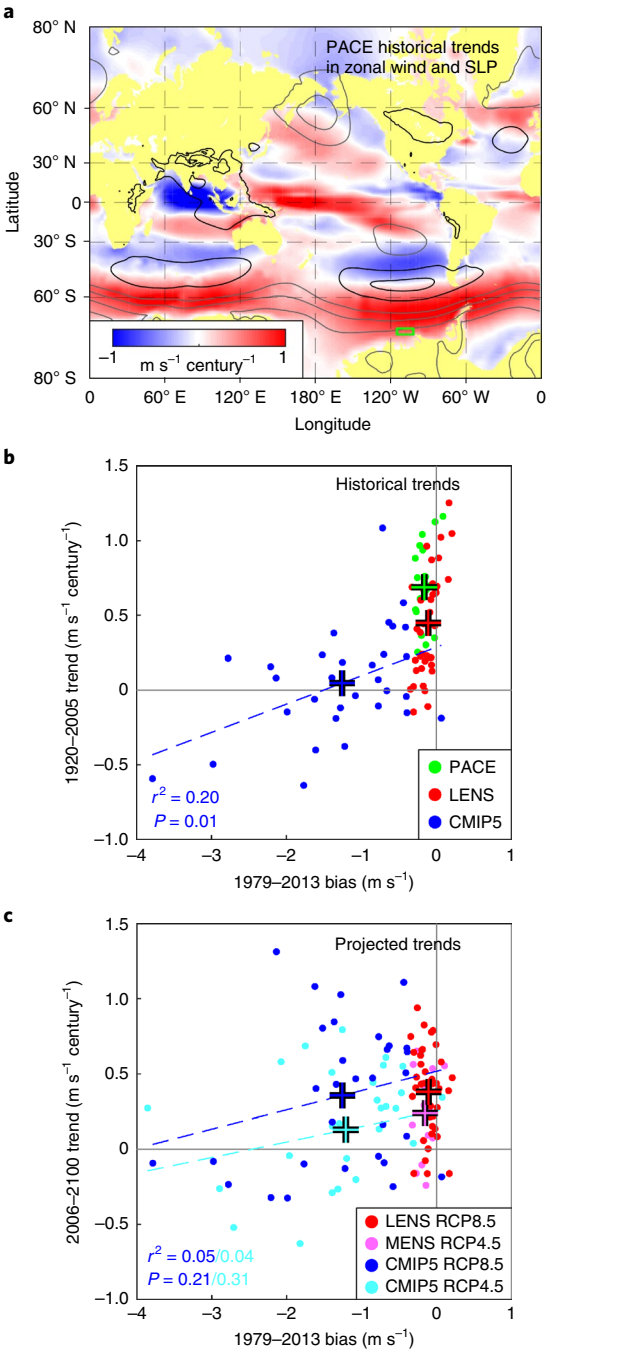

Fig. 4 | Trends in Amundsen Sea winds within climate model ensembles. **a**, The 1920–2005 trends in the PACE ensemble mean. Colours (contours) show trend in zonal winds (SLP). Contours have a spacing of 0.5 hPa century^{-1}, with black positive, grey negative and the zero contour omitted. **b**,**c**, Historical (**b**) and projected (**c**) PITT wind trends versus present-day bias (mean model zonal wind minus mean ERA-Interim zonal wind). Ensemble-mean values are shown by + symbols. The ensemble regression of CMIP5 historical trends shows that the larger LENS trend is consistent with its smaller bias. There is no dependence of CMIP5 projected trends on present-day bias.

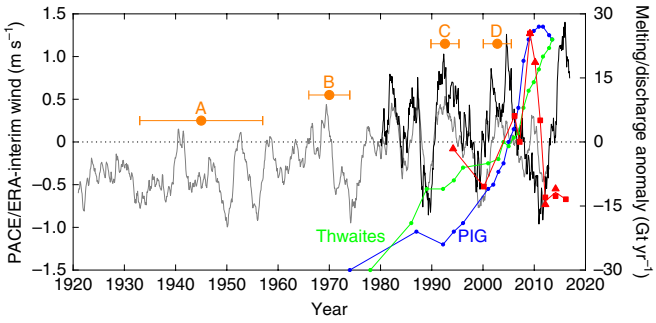

Fig. 5 | One century of wind forcing and ice-sheet response. Grey and black show PACE ensemble-mean and ERA-Interim winds, respectively. Green and blue show anomalies in discharge of Thwaites Glacier and PIG[3], relative to 102 and 108 Gt yr^{-1} median values, respectively. Red shows anomalies in combined melt rates from PIG[5] (triangles) and the Dotson Ice Shelf[6] (squares), relative to a median of 48 Gt yr^{-1}. Orange events include initial (A) and final (B) ungrounding of PIG from a submarine ridge[8,12], and the onset of recent thinning of Pine Island (C) and Thwaites (D) glaciers[4] (mean ± 1 s.d. of dates for tributaries).

Owing to the unpredictable phasing of internal climate variability, there is significant variance in wind trends between ensemble members, with the 1 s.d. range for LENS and MENS extending between no trend and twice the mean trend (Supplementary Fig. 6). Internal variability is therefore of comparable importance to radiative forcing in determining the magnitude of PITT wind changes during the twenty-first century. In the CMIP5 ensembles, inter-model differences add further uncertainty to the future trajectory of PITT winds (Supplementary Fig. 6). To deliver meaningful projections of the WAIS over this period, ice-sheet models will need to adopt an ensemble approach forced by multiple realizations of ocean melting.

Online content

Any methods, additional references, Nature Research reporting summaries, source data, statements of code and data availability and associated accession codes are available at https://doi.org/10.1038/s41561-019-0420-9.

Received: 13 December 2018; Accepted: 26 June 2019;
Published online: 12 August 2019

References

1. Shepherd, A. et al. Mass balance of the Antarctic Ice Sheet from 1992 to 2017. *Nature* **558**, 219–222 (2018).
2. Shepherd, A., Wingham, D. & Rignot, E. Warm ocean is eroding West Antarctic Ice Sheet. *Geophys. Res. Lett.* **31**, L23402 (2004).
3. Mouginot, J., Rignot, E. & Scheuchl, B. Sustained increase in ice discharge from the Amundsen Sea Embayment, West Antarctica, from 1973 to 2013. *Geophys. Res. Lett.* **41**, 1576–1584 (2014).
4. Konrad, H. et al. Uneven onset and pace of ice-dynamical imbalance in the Amundsen Sea Embayment, West Antarctica. *Geophys. Res. Lett.* **44**, 910–918 (2017).
5. Jenkins, A. et al. Decadal ocean forcing and Antarctic Ice Sheet response: lessons from the Amundsen Sea. *Oceanography* **29**, 106–117 (2016).
6. Jenkins, A. et al. West Antarctic Ice Sheet retreat in the Amundsen Sea driven by decadal oceanic variability. *Nat. Geosci.* **11**, 733–738 (2018).
7. Snow, K. et al. The response of ice sheets to climate variability. *Geophys. Res. Lett.* **44**, 11878–11885 (2017).
8. Jenkins, A. et al. Observations beneath Pine Island Glacier in West Antarctica and implications for its retreat. *Nat. Geosci.* **3**, 468–472 (2010).
9. Steig, E. J., Ding, Q., Battisti, D. S. & Jenkins, A. Tropical forcing of Circumpolar Deep Water inflow and outlet glacier thinning in the Amundsen Sea Embayment, West Antarctica. *Ann. Glaciol.* **53**, 19–28 (2012).
10. De Rydt, J., Holland, P. R., Dutrieux, P. & Jenkins, A. Geometric and oceanographic controls on melting beneath Pine Island Glacier. *J. Geophys . Res. Oceans* **119**, 2420–2438 (2014).
11. De Rydt, J. & Gudmundsson, G. H. Coupled ice shelf–ocean modeling and complex grounding line retreat from a seabed ridge. *J. Geophys. Res. Earth Surf.* **121**, 865–880 (2016).
12. Smith, J. A. et al. Sub-ice-shelf sediments record history of twentieth-century retreat of Pine Island Glacier. *Nature* **541**, 77–80 (2016).
13. Jacobs, S. S., Hellmer, H. H. & Jenkins, A. Antarctic Ice Sheet melting in the Southeast Pacific. *Geophys. Res. Lett.* **23**, 957–960 (1996).
14. Dutrieux, P. et al. Strong sensitivity of Pine Island ice-shelf melting to climatic variability. *Science* **343**, 174–178 (2014).
15. Thoma, M., Jenkins, A., Holland, D. & Jacobs, S. Modelling Circumpolar Deep Water intrusions on the Amundsen Sea continental shelf, Antarctica. *Geophys. Res. Lett.* **35**, L18602 (2008).
16. Kimura, S. et al. Oceanographic controls on the variability of ice-shelf basal melting and circulation of glacial meltwater in the Amundsen Sea Embayment, Antarctica. *J. Geophys. Res. Oceans* **122**, 10131–10155 (2017).
17. Webber, B. G. M., Heywood, K. J., Stevens, D. P. & Assmann, K. M. The impact of overturning and horizontal circulation in Pine Island Trough on ice shelf melt in the Eastern Amundsen Sea. *J. Phys. Oceanogr.* **49**, 63–83 (2019).
18. Assmann, K. M. et al. Variability of Circumpolar Deep Water transport onto the Amundsen Sea continental shelf through a shelf break trough. *J. Geophys. Res. Oceans* **118**, 6603–6620 (2013).
19. Walker, D. P., Jenkins, A., Assmann, K. M., Shoosmith, D. R. & Brandon, M. A. Oceanographic observations at the shelf break of the Amundsen Sea, Antarctica. *J. Geophys. Res. Oceans* **118**, 2906–2918 (2013).
20. St-Laurent, P., Klinck, J. M. & Dinniman, M. S. Impact of local winter cooling on the melt of Pine Island Glacier, Antarctica. *J. Geophys. Res. Oceans* **120**, 6718–6732 (2015).
21. Davis, P. E. D. et al. Variability in basal melting beneath Pine Island Ice Shelf on weekly to monthly timescales. *J. Geophys. Res. Oceans* **123**, 8655–8669 (2018).
22. Webber, B. G. M. et al. Mechanisms driving variability in the ocean forcing of Pine Island Glacier. *Nat. Commun.* **8**, 14507 (2017).
23. Kim, T. W. et al. Is Ekman pumping responsible for the seasonal variation of warm Circumpolar Deep Water in the Amundsen Sea? *Cont. Shelf Res.* **132**, 38–48 (2017).
24. Raphael, M. N. et al. The Amundsen Sea Low: variability, change, and impact on Antarctic climate. *Bull. Am. Meteorol. Soc.* **97**, 111–121 (2016).
25. Lachlan-Cope, T. & Connolley, W. Teleconnections between the tropical Pacific and the Amundsen–Bellinghausens Sea: role of the El Niño/Southern Oscillation. *J. Geophys. Res. Atmos.* **111**, D23101 (2006).
26. Deser, C., Alexander, M. A., Xie, S. P. & Phillips, A. S. Sea surface temperature variability: patterns and mechanisms. *Annu. Rev. Mar. Sci.* **2**, 115–143 (2010).
27. Schneider, D. P. & Deser, C. Tropically driven and externally forced patterns of Antarctic sea ice change: reconciling observed and modeled trends. *Clim. Dyn.* **50**, 4599–4618 (2018).
28. Steig, E. J. et al. Recent climate and ice-sheet changes in West Antarctica compared with the past 2,000 years. *Nat. Geosci.* **6**, 372–375 (2013).
29. Schneider, D. P. & Steig, E. J. Ice cores record significant 1940s Antarctic warmth related to tropical climate variability. *Proc. Natl Acad. Sci. USA* **105**, 12154–12158 (2008).
30. Kay, J. E. et al. The Community Earth System Model (CESM) Large Ensemble Project: a community resource for studying climate change in the presence of internal climate variability. *Bull. Am. Meteorol. Soc.* **96**, 1333–1349 (2015).
31. Bracegirdle, T. J., Turner, J., Hosking, J. S. & Phillips, T. Sources of uncertainty in projections of 21st century westerly wind changes over the Amundsen Sea, West Antarctica, in CMIP5 climate models. *Clim. Dyn.* **43**, 2093–2104 (2014).
32. Harvey, B. J., Shaffrey, L. C. & Woollings, T. J. Equator-to-pole temperature differences and the extra-tropical storm track responses of the CMIP5 climate models. *Clim. Dyn.* **43**, 1171–1182 (2014).
33. Arblaster, J. M. & Meehl, G. A. Contributions of external forcings to southern annular mode trends. *J. Clim.* **19**, 2896–2905 (2006).
34. Schneider, D. P., Deser, C. & Fan, T. T. Comparing the impacts of tropical SST variability and polar stratospheric ozone loss on the Southern Ocean westerly winds. *J. Clim.* **28**, 9350–9372 (2015).
35. Gillett, N. P., Fyfe, J. C. & Parker, D. E. Attribution of observed sea level pressure trends to greenhouse gas, aerosol, and ozone changes. *Geophys. Res. Lett.* **40**, 2302–2306 (2013).
36. Yeh, S. W. et al. ENSO atmospheric teleconnections and their response to greenhouse gas forcing. *Rev. Geophys.* **56**, 185–206 (2018).
37. Cai, W. J. et al. ENSO and greenhouse warming. *Nat. Clim. Change* **5**, 849–859 (2015).
38. Christianson, K. et al. Sensitivity of Pine Island Glacier to observed ocean forcing. *Geophys. Res. Lett.* **43**, 10817–10825 (2016).

39. Rignot, E., Jacobs, S., Mouginot, J. & Scheuchl, B. Ice-shelf melting around Antarctica. *Science* **341**, 266–270 (2013).
40. Barnes, E. A., Barnes, N. W. & Polvani, L. M. Delayed Southern Hemisphere climate change induced by stratospheric ozone recovery, as projected by the CMIP5 models. *J. Clim.* **27**, 852–867 (2014).
41. Sanderson, B. M., Oleson, K. W., Strand, W. G., Lehner, F. & O'Neill, B. C. A new ensemble of GCM simulations to assess avoided impacts in a climate mitigation scenario. *Climatic Change* **146**, 303–318 (2018).
42. Little, C. M. & Urban, N. M. CMIP5 temperature biases and 21st century warming around the Antarctic coast. *Ann. Glaciol.* **57**, 69–78 (2016).

Acknowledgements

We are grateful to the originators of the many open-access datasets synthesized in this study, including remotely sensed sea-ice data, atmospheric reanalysis model results, sea surface temperature and bathymetry observations, derived climate indices, and many climate model simulations. P.D. was supported by NSF awards 1643285 and 1644159. E.J.S. was supported by NSF award 1602435.

Author contributions

P.R.H. conceived the study and led the data processing. T.J.B. processed the CMIP5 model results. All authors discussed the results and implications and collaborated on writing the manuscript at all stages.

Competing interests

The authors declare no competing interests.

Additional information

Supplementary information is available for this paper at https://doi.org/10.1038/s41561-019-0420-9.

Reprints and permissions information is available at www.nature.com/reprints.

Correspondence and requests for materials should be addressed to P.R.H.

Publisher's note: Springer Nature remains neutral with regard to jurisdictional claims in published maps and institutional affiliations.

Methods

Observational datasets. The total-surface-stress formulae employ daily ice concentration[43] and drift[44] data derived from passive microwave satellite data, and surface winds from the ECMWF ERA-Interim[45]. The results are set in context using the Bedmap2 seabed dataset[46]. The stress calculation is detailed below.

The variability of 10 m zonal winds and surface stresses in the Amundsen Sea are considered over a PITT box extending over 115°–102° W, 71.8°–70.2° S (Fig. 1). This box is focused on the shelf-break mouths of the troughs feeding PIG and Thwaites Glacier, and is therefore both farther south and smaller than that used by other authors[5,6,9,14,15,31]. The box used by these previous authors was chosen to reflect the coarser resolution of an earlier reanalysis dataset[15]. These PITT winds are set in their wider context using global SST data from the Extended Reconstructed SST (ERSST) v5 dataset[47], and global SLP from ERA-Interim. Throughout the paper, the term 'eastward' is used to refer to wind anomalies oriented in the eastward direction, while the term 'westerly' is used to refer to a wind that is actually blowing from west to east in absolute terms.

Calculation of surface stresses. The 'total' surface stress ($\boldsymbol{\tau}$) is calculated simply as the sum of air–ocean ($\boldsymbol{\tau}_a$) and ice–ocean ($\boldsymbol{\tau}_i$) stresses, weighted by ice concentration (C):

$$\boldsymbol{\tau} = (1 - C)\boldsymbol{\tau}_a + C\boldsymbol{\tau}_i$$

The individual stresses are represented as

$$\boldsymbol{\tau}_a = \rho_a c_a |\mathbf{u}_a| \mathbf{u}_a$$

$$\boldsymbol{\tau}_i = \rho_o c_o |\mathbf{u}_i| \mathbf{u}_i$$

where $\mathbf{u}_a$ is the 10 m wind vector, $\mathbf{u}_i$ is the observed ice drift vector, $\rho_a = 1.3\,\mathrm{kg\,m^{-3}}$ and $\rho_o = 1{,}030\,\mathrm{kg\,m^{-3}}$ are air and ocean densities, and $c_a = 0.001$ and $c_o = 0.006$ are air and ocean drag coefficients, respectively.

This formulation is perhaps the simplest conceivable. There are many alterations that could be adopted[23], such as including the ocean surface current, adopting an air–ocean stress formulation that accounts for sea state, or attempting to represent spatial and temporal variation in drag coefficients. These alternatives are not pursued because their requirement for additional unknown quantities implies they may not lead to a more realistic stress. In particular, including ocean currents in the stress calculation could radically alter the results[16], but suitable current observations are not available. Our approach should be regarded as a simple first attempt to examine nominal total stresses to build understanding of the role of sea ice.

Ekman pumping by the total and wind-only stresses are calculated according to

$$w\mathbf{k} = \frac{\nabla \times \boldsymbol{\tau}}{\rho_o f}$$

$$w_a\mathbf{k} = \frac{\nabla \times \boldsymbol{\tau}_a}{\rho_o f}$$

where $\mathbf{k}$ is the vertical unit vector, w is the total Ekman pumping, w_a is the wind-only Ekman pumping, and $f = -1.4 \times 10^{-4}\,\mathrm{s^{-1}}$ is the Coriolis parameter.

The above formulae employ daily ice concentration and drift data and reanalysis model winds. All datasets are used for 1992–2016, the period during which consistent passive microwave data are available, and are binned/interpolated to a 25-km-resolution polar stereographic grid, on which stresses are calculated. The stresses are smoothed spatially with a 3 × 3 grid cell mean to remove gridding artefacts manifested in the Ekman pumping fields. The vector correlation between total and wind-only stresses is calculated according to a technique that measures covariance in both magnitude and direction[48].

Anomalies in the wind-only stress and total stress have a complex relationship on-shelf (Supplementary Fig. 1). Their correlation drops near coasts because the ice strength resists convergence and shear. However, there are also significant polynyas on-shelf, where mobile ice permits a higher stress[23,49] that is better correlated to winds. The largest is the Amundsen Sea Polynya, which forms in the lee of icebergs grounded on a ridge north of Bear Island[50]. Shearing of mobile polynya ice against pack ice to the northeast creates Ekman upwelling[23,49]. Similar features occur west of Siple Island and Grant Island, which also host grounded icebergs[50]. Accounting for sea ice strongly affects the Ekman pumping. Ekman pumping is generally weak, with interannual variability of only ~5 m yr^{-1}, suggesting that it cannot account for the large variations of CDW layer thickness that govern melting[6,14]. Therefore, we focus on variations in CDW import to the shelf driven directly by zonal stress anomalies at the shelf break[5,18,19]. Accounting for sea ice has little effect on zonal stress anomalies at the shelf break, so zonal winds are used as a proxy for zonal stress at the shelf break throughout the study.

Climate indices. The linkage between Amundsen Sea winds and a broad range of climatic indices (https://www.esrl.noaa.gov/psd/data/climateindices/list/) are considered, but the SOI and IPO are particularly emphasized. All measures of ENSO and Pacific decadal variability are correlated so the choice is not of crucial importance; the two chosen indices are most highly correlated with PITT winds (Supplementary Fig. 4).

The SOI (http://www.cpc.ncep.noaa.gov/data/indices/soi) is a measure of ENSO variability. It is derived from the SLP difference between Tahiti and Australia (Fig. 3c), a measure of anomalous atmospheric convection over the tropical Pacific. The SOI is positive during La Niña conditions, so we consider –SOI to align the index with the other measures considered.

The tripole IPO index (https://www.esrl.noaa.gov/psd/data/timeseries/IPOTPI/) is a measure of decadal variability in the Pacific climate system. This variability resembles ENSO but acts on longer timescales, features a different spatial pattern and involves a variety of climate processes[51–53]. Pacific decadal variability has been characterized in several ways, for example, as the second principal component (PC2) of monthly Pacific SST anomalies after a 13 yr low-pass filter (PC1 being global warming)[54]. The 'tripole' index employed here uses the SST anomaly between three areas of the tropical and subtropical Pacific (Fig. 2d) to represent the pattern of the associated empirical orthogonal function and thus can be used to approximate the PC[54]. This index can be considered monthly (unfiltered), or subjected to a 13 yr low-pass filter to recover decadal variability similar to that of the original PC. The unfiltered index represents the monthly variability that underlies the decadal variability.

Significance of time series correlations. Several figures involve the calculation of correlations between time series. These correlations are calculated on detrended time series at zero lag, after the application of a 2 yr running mean. Owing to the use of a 2 yr running mean throughout this study, the effective number of degrees of freedom in these correlations is relatively small for the 1979–2017 period used in Fig. 2 and Supplementary Figs. 3 and 4. The effective sample size was analysed, accounting for autocorrelation[55], and in all cases was found to be very close to $Y/2$, where Y is the number of years in the record. This is the expected result for time series subjected to a 2 yr running mean that have negligible autocorrelation on timescales longer than 2 yr. Therefore, we derived the statistical significance of the correlations using a 2-sided t-test with $Y/2$ as the degrees of freedom.

Climate model simulations. We examine Amundsen Sea winds in climate model simulations, including the CMIP5 archive[31], the CESM LENS[30], CESM MENS[41] and CESM PACE[56]. CMIP5 data were obtained from the Centre for Environmental Data Analysis (http://www.ceda.ac.uk/), while the CESM simulations were obtained from the National Center for Atmospheric Research Climate Data Gateway (https://www.earthsystemgrid.org/). The ensembles used are summarized in Supplementary Table 1.

For the ensemble of CMIP5 simulations, the models and processing follow an earlier study[31]. Data were assessed from 'historical' forcing simulations from 1920–2005 and future projections using RCP4.5 and RCP8.5 from 2006–2100. We include only the first simulation from each different model to ensure the models are weighted equally, totalling 30 (31) realizations of RCP4.5 (RCP8.5). The historical ensemble includes the 31 simulations that continue to the RCP8.5 projection. RCP4.5 features a radiative forcing that stabilizes in 2100, while RCP8.5 represents a continually increasing forcing. In both scenarios, stratospheric ozone recovers to near pre-ozone hole levels by 2100. For each scenario, the spread between ensemble members reflects a combination of both model uncertainty and internal climate variability. By comparing the projected trends in the two ensembles, we are able to determine the influence of future radiative forcing on PITT winds.

The LENS ensemble comprises 40 simulations of the CESM1.1 coupled climate model, in which the atmosphere, sea ice and ocean models have a resolution of ~1° (ref. [30]). Each simulation represents the period 1920–2100, using 'historical' forcings until 2005 and RCP8.5 afterwards. The CESM and its direct ancestors are not included in the CMIP5 ensemble analysed here. The only difference between LENS ensemble members is a random machine-precision (10^{-14} °C) perturbation to the initial atmospheric temperature, which rapidly grows in the chaotic climate system. Since the model physics are identical in all simulations, the spread between ensemble members represents only the influence of random internal climate variability.

The MENS ensemble comprises 15 simulations of the same model as LENS. MENS simulations are identical to LENS in every way apart from the projected radiative forcing, which follows RCP4.5 instead of RCP8.5. MENS simulations branch from the first 15 members of LENS in 2006, running until 2080. Comparing MENS and LENS reveals the influence of radiative forcing scenario on PITT winds within the CESM model. This offers additional information to the CMIP5 comparison because the CESM model has exceptionally low bias, and the difference between ensemble members is caused only by internal climate variability, free from the influence of model structural difference.

One complication is that MENS simulations only run until 2080, rather than 2100 in the other ensembles. Supplementary Tables 2 and 3 report LENS ensemble metrics for both the period to 2080 and 2100, for ease of comparison to MENS. The LENS trends are larger over the longer period, and their difference to MENS more significant. However, we have no way of knowing how MENS would evolve after 2080, so in the main paper we rely on the 2006–2080 trends,

for which the difference between LENS and MENS ensembles is not statistically significant (Supplementary Table 3). This is partly a result of the relatively small size of MENS.

The PACE ensemble comprises 20 historical simulations (1920–2013) of the CESM1.1 model, in which eastern tropical Pacific SSTs are constrained to follow their observed history[56]. The restoring imposes SST anomalies in the region between 15°S to 15°N and 180°W to the coast of the Americas, plus a restoring ramp-down region of 5° to the north, south and west[57]. The restoring replaces model temporal SST anomalies with observed temporal SST anomalies. Therefore, to a first approximation, the restoring does not alter any mean-state bias in the climate model. The non-conservation of heat induced by the restoring is typically smaller than both the top-of-atmosphere radiation imbalance, and its model ensemble spread[58]. PACE simulations use historical forcings for 1920–2005 and RCP8.5 forcings for 2006–2013. The models used in the LENS and PACE ensembles are structurally identical. The forcing of the two ensembles is also identical apart from the representation of ozone depletion, which is derived from different datasets in the two ensembles[27]. This difference in ozone forcing has some effect on stratospheric temperatures, but no discernible effect on the surface winds that are the focus of this study[34]. This is evident from the absence of any noticeable signature of ozone depletion in the tropical response (the mean difference between PACE and LENS; see below) in Fig. 3b. Since all PACE ensemble members have identical model structure and are constrained to follow the observed history of eastern and central tropical Pacific SST anomalies, the spread between PACE ensemble members represents internal climate variability that is associated with SSTs outside this region.

Interpretation of climate model results. The real climate trajectory combines the effects of a single realization of random internal climate variability with a response to external forcings (greenhouse gases, ozone, aerosols, land use, volcanoes, solar). Therefore, it should be most comparable to an individual member from our ensembles. However, model representations of the climate system are imperfect. The value of our model ensembles is therefore in helping to distinguish the effects of forcing, internal variability and model uncertainty.

The CMIP5 ensemble spread represents both model uncertainty and internal climate variability. The LENS and MENS ensemble spread represents only internal variability. The PACE ensemble spread represents only internal variability associated with regions outside the eastern tropical Pacific. The CMIP5, LENS and MENS ensemble means are derived by averaging over multiple realizations of random internal climate variability, and therefore represent estimates of the climate response to external forcings. These estimates differ in that the CMIP5 ensemble mean includes model uncertainty in the forced response, while the LENS and MENS ensemble means more accurately estimate the forced response of a single model. The PACE ensemble mean estimates the combined effect of the forced response and the real variability associated with the observed trajectory of tropical Pacific SSTs.

The influence of Pacific variability on the historical PITT wind trend can be deduced from differences between PACE and LENS. There are significant summer and autumn trends in both ensembles, while only PACE has trends in winter and spring (Supplementary Table 2). As a result, the PACE annual trend is higher than that of LENS (Table 1 and Supplementary Fig. 6). This difference between PACE and LENS mean trends is significant at the 95% confidence level for annual trends and for winter and spring (Supplementary Table 3), suggesting that Pacific variability made a small but detectible enhancement to the radiatively forced trend during the twentieth century.

Since the PACE and LENS ensembles use the same model, their response to external forcing should in principle be the same. Therefore, we define the LENS ensemble mean as representing the 'forced response' in both the LENS and PACE ensembles. We may then subtract the LENS ensemble mean from the PACE ensemble mean to isolate the 'tropical response'[27]. This tropical response is an estimate of the unforced variability in the climate system that is associated with tropical Pacific SSTs. The crucial advantage in this approach is that it allows us to consistently compare the magnitude of climate responses (for example, PITT winds) to external forcing (forced response) and tropical Pacific variability (tropical response). Tropical response winds closely follow the unfiltered IPO index (Fig. 3b), clarifying the causality of the linkage. When tropical Pacific SSTs are prescribed, PITT winds covary with the whole-Pacific SST pattern that results (hence they vary with the unfiltered IPO index). Since the unfiltered IPO index represents variability that underlies decadal variability on filtering, this implies that PITT winds follow the decadal variability of the IPO.

There are several caveats to the interpretation of the tropical response. First, the approach assumes that the forced and tropical responses are linearly separable, thus neglecting the role of external forcing on tropical variability. Second, the LENS and PACE ensembles have different ozone forcing, which could contaminate the tropical response, though the impact of this difference on surface winds is known to be small[34], and our results support this (Fig. 3b). Third, the forced response in the LENS and PACE ensembles may actually differ, since the restoring in the latter alters the SST trend within the restoring region[58]. Ultimately, however, the results of many studies show that the 'tropical response' concept realistically and usefully depicts the influence of tropical Pacific variability[27].

Amundsen Sea ice-shelf melting time series. Figure 5 shows a time series of ice-shelf melt rates derived from ocean observations near PIG[5,14] and DIS[6]. Including both ice shelves offers improved temporal coverage, since most oceanographic surveys sampled only one of the two ice fronts. While the two ice shelves occupy distinct seabed troughs, and differ in the details of their geometry and oceanographic forcing, the phasing of their interannual variability is coherent and thought to be driven by common shelf-break wind forcing[5,6,14,16]. The derivation of melt rates for each ice shelf is fully documented in the original papers[6,14], and only their combination requires further explanation here.

To display a consistent time series, we scale the DIS melt rates to produce an approximate PIG-equivalent melt rate. The scaling is derived from three years that have melt rates for both cavities (2009, 2012, 2014), which fortuitously includes the maximum and minimum observed melt rates for both cavities. PIG-equivalent DIS melt rates are derived by regressing PIG melt rates against DIS melt rates for these three years, yielding

$$m_{\mathrm{PIGeq}} = 23.9 + 0.54\, m_{\mathrm{DIS}}$$

where all values are in Gt yr^{-1}. These PIG-equivalent DIS melt rates are then combined with unscaled PIG melt rates to create the melt time series. The mean of the two melt values is used for years where both cavities were sampled. The combination of the two cavities is based on only three common years and is therefore offered only for illustrative purposes. Nevertheless, the combined time series offers a credible account of decadal variability in the Amundsen Sea that is consistent with the independent ERA-Interim winds (Fig. 5).

Data availability

Sea-ice concentration and drift data that support the findings of this study are available from the National Snow and Ice Data Center (https://doi.org/10.5067/8GQ8LZQVL0VL and https://doi.org/10.5067/O57VAIT2AYYY, respectively). ERA-Interim reanalysis data are available from the ECMWF (https://apps.ecmwf.int/datasets/data/interim-full-daily). Extended Reconstructed Sea Surface Temperature data are available from the National Oceanic and Atmospheric Administration National Climatic Data Center (https://www.ncdc.noaa.gov/data-access/marineocean-data/extended-reconstructed-sea-surface-temperature-ersst-v5). Seabed data are available from the British Antarctic Survey (https://secure.antarctica.ac.uk/data/bedmap2). Climate indices are available from the National Oceanic and Atmospheric Administration Earth System Research Laboratory (https://www.esrl.noaa.gov/psd/data/climateindices/list). CMIP5 simulation data are available from the Centre for Environmental Data Analysis (http://www.ceda.ac.uk). CESM simulation data are available from the National Center for Atmospheric Research Climate Data Gateway (https://www.earthsystemgrid.org).

Code availability

The Matlab scripts used for the analyses described in this study can be obtained from the corresponding author on reasonable request.

References

43. Cavalieri, D. J., Parkinson, C. L., Gloersen, P. & Zwally, H. J. *Sea Ice Concentrations from Nimbus-7 SMMR and DMSP SSM/I-SSMIS Passive Microwave Data, Version 1. 1992–2016* (National Snow and Ice Data Center, 1996); https://doi.org/10.5067/8GQ8LZQVL0VL
44. Tschudi, M., Fowler, C., Maslanik, J., Stewart, J. S. & Meier, W. *Polar Pathfinder Daily 25km EASE-Grid Sea Ice Motion Vectors, Version 3. 1992–2016* (National Snow and Ice Data Center, 2016); https://doi.org/10.5067/O57VAIT2AYYY
45. Dee, D. P. et al. The ERA-Interim reanalysis: configuration and performance of the data assimilation system. *Q. J. R. Meteorol. Soc.* **137**, 553–597 (2011).
46. Fretwell, P. et al. Bedmap2: improved ice bed, surface and thickness datasets for Antarctica. *Cryosphere* **7**, 375–393 (2013).
47. Huang, B. et al. *NOAA Extended Reconstructed Sea Surface Temperature (ERSST). Version 5. 1854–2016* (NOAA National Centers for Environmental Information, 2017); https://www.ncdc.noaa.gov/data-access/marineocean-data/extended-reconstructed-sea-surface-temperature-ersst-v5
48. Crosby, D. S., Breaker, L. C. & Gemmill, W. H. A proposed definition for vector correlation in geophysics—theory and application. *J. Atmos. Ocean. Technol.* **10**, 355–367 (1993).
49. Kim, C. S. et al. Variability of the Antarctic Coastal Current in the Amundsen Sea. *Estuar. Coast. Shelf Sci.* **181**, 123–133 (2016).
50. Mazur, A. K., Wåhlin, A. K. & Krezel, A. An object-based SAR image iceberg detection algorithm applied to the Amundsen Sea. *Remote Sens. Environ.* **189**, 67–83 (2017).
51. Zhang, Y., Wallace, J. M. & Battisti, D. S. ENSO-like interdecadal variability: 1900–93. *J. Clim.* **10**, 1004–1020 (1997).
52. Power, S., Casey, T., Folland, C., Colman, A. & Mehta, V. Inter-decadal modulation of the impact of ENSO on Australia. *Clim. Dyn.* **15**, 319–324 (1999).

53. Newman, M. et al. The Pacific Decadal Oscillation, revisited. *J. Clim.* **29**, 4399–4427 (2016).
54. Henley, B. J. et al. A tripole index for the Interdecadal Pacific Oscillation. *Clim. Dyn.* **45**, 3077–3090 (2015).
55. Bretherton, C. S., Widmann, M., Dymnikov, V. P., Wallace, J. M. & Blade, I. The effective number of spatial degrees of freedom of a time-varying field. *J. Clim.* **12**, 1990–2009 (1999).
56. Deser, C., Guo, R. X. & Lehner, F. The relative contributions of tropical Pacific sea surface temperatures and atmospheric internal variability to the recent global warming hiatus. *Geophys. Res. Lett.* **44**, 7945–7954 (2017).
57. Kosaka, Y. & Xie, S. P. Recent global-warming hiatus tied to equatorial Pacific surface cooling. *Nature* **501**, 403–407 (2013).
58. Kosaka, Y. & Xie, S. P. The tropical Pacific as a key pacemaker of the variable rates of global warming. *Nat. Geosci.* **9**, 669–673 (2016).